Detailed Atomistic Simulation of Oriented Pseudocrystalline Polymers and Application to a Stiff-Chain Aramid

G. C. Rutledge and U. W. Suter*

Department of Chemical Engineering, Massachusetts Institute of Technology, Cambridge, Massachusetts 02139, and Institut für Polymere, Eidgenössische Technische Hochschule, CH-8092 Zürich, Switzerland

Received June 28, 1990; Revised Manuscript Received October 9, 1990

ABSTRACT: Atomistic modeling methods are applied to the study of microstructure formation in the solid state of a highly ordered polymer. The calculations are adapted to the consideration of local structural imperfections, with retention of the long-range crystalline contribution to structure compaction and cohesive energy. The simulation technique employs no adjustable parameters and incorporates the simultaneous minimization of total potential energy with respect to both intramolecular and intermolecular degrees of freedom. The method is applied to the analysis of the solid state of the rigid-rod polymer poly(*p*-phenyleneterephthalamide). The simulation results, based solely on a potential energy criterion, suggest that such rodlike polymers may realize local helix distortions and multiple packing geometries of chains as a consequence of the substantial magnitude of intermolecular forces in effect, in conjunction with a disparity in the specificity of interactions in the different spatial directions. However, all predicted structures possess the common features of chain extension and hydrogen-bonded sheet formation, with polymorphism hinging primarily on the nature of packing between sheets.

I. Introduction

The methods of molecular mechanics and molecular dynamics have proven considerably useful in the correlation of macroscopic behavior with atomic-level structural detail. Usually, these methods are employed to obtain atomic potential energy functions in systems of experimentally known structure or, conversely, to elucidate the characteristics of a previously identified region of phase space. The methods prove especially useful in those instances where simplifying assumptions, such as independent behavior of single molecules, structural periodicity, or idealized stochastic disorder, are both realistic and quantifiable. Applications to isolated macromolecules,[1-7] low molecular weight crystals,[8,9] and disordered liquids[10,11] are relatively numerous. However, the detailed treatment of atomic-level interactions and chain packing of macromolecules at glass and crystal densities are considerably fewer.

Glasses of atactic vinyl polymers[12,13] and crystals of flexible-chain aliphatic polymers,[14-23] representing the extremes of disorder and regularity in the solid state, have received attention from atomistic simulations in the past. In most of the latter cases, the problems associated with the possibly antagonistic criteria determining the single-chain conformation and the regularity of the crystal structure are assumed to be decoupled as a result of chain pliancy. In these cases, investigators usually treat the crystallite domain through the use of periodicity simplifications appropriate only to the ideal crystal, or even impose a given crystal symmetry based on experimental observations. However, in the solid state of less flexible polymers, one encounters an environment that is both conformationally constrained and densely packed. The close packing and unusually high intermolecular energies realized in the relatively dense solid state of rigid-rod polyamides create a condition for considerable influence of intermolecular parameters on local chain conformation, which in turn must readjust to accommodate nearest-neighbor interactions. As a result, one must anticipate nonideal or pseudocrystalline structures whose preferred organizations cannot realize perfect translational periodicity over long distances but may exhibit conformational helix discommensurations of the type suggested by Saruyama,[24,25] with energies comparable to the large intermolecular energies operative in the chain packing. One may further anticipate that intermolecular interactions between nonuniform helices or helices possessing some form of constitutional disorder would lead to anomalous packing behavior between neighboring chain segments.

In this paper we present a static atomistic modeling technique aimed specifically at the simulation of such potentially pseudocrystalline materials without resort to the use of adjustable parameters. We employ a conformation-dominated chain-building technique and a packing method that is amenable to the inclusion of nonrational or incommensurate helices. Energy calculation is composed of two parts, the predominant term of which focuses on the short-range distortion effects characteristic of local chain packing, with the superposition of a correction term that assumes perfect crystal periodicities to reflect the compressive effects of longer range interactions. Energy minimization is simultaneous with respect to both intramolecular and intermolecular degrees of freedom, a feature that is critical to the realistic modeling of the cooperative interactions between atoms in multichain systems. We then discuss a procedure by which we use this technique to scan all of configuration space as a tool not only to elucidate structural detail in regions of a priori interest but also to identify regions not considered before. Finally, the method is applied to the study of poly(*p*-phenyleneterephthalamide) (PPTA), a stiff-chain polymer whose chemistry and solid-state properties are of current scientific and commercial interest and the nature of the crystallinity of which has been the subject of some discussion in the literature. The results of this analysis are compared with literature and experimental results in a companion paper.

II. Atomistic Simulation of Ordered Structure

General Approach. The static atomistic modeling methodology assumes that the energy of the material in question may be calculated from a set of force interactions,

* To whom correspondence should be addressed at the Institut für Polymere, Eidgenössische Technische Hochschule.

0024-9297/91/2224-1921$02.50/0

corresponding to a total potential energy characteristic of the structure. It is composed of two fundamental parts: (1) a method for representation of the material as an ensemble of atoms, or atomic groups; (2) a realistic representation of the forces operating between individual members of the ensemble. In the ideal crystal representation, the first is defined completely throughout space by the local coordinates of the conformational repeat unit, in conjunction with transformations required to describe symmetry-related elements within the unit cell and the three periodicity vectors that define the replication of the unit cell in space. This periodicity may also be used to simplify the calculation of interatomic interactions, as will be described later. The approach that follows begins with the determination of the conformation behavior of the single chain, as prescribed by intramolecular interactions. From the single chain an explicit multichain structure is generated that reflects short-range intermolecular interactions in the nearest-neighbor and next-nearest-neighbor shells. Periodicity simplifications are invoked only to estimate the appropriate long-range compaction forces. The calculations assume that the force interactions may be realistically represented by empirical bond length, bond angle, and bond torsion deformation functions and additive two-body interactions in the case of nonbonded species or intramolecular pairs whose interaction distance is conformationally dependent. Iterations along a decreasing potential energy trajectory are performed by using a quasi-Newton algorithm with simultaneous variation of all intramolecular and intermolecular degrees of freedom.

Structural Representation. Chain Generation and Helix Alignment. The generation of the representative chain involves the specification of the set of three-dimensional coordinates locating the atoms or rigid moieties that comprise the chain and entails $3n - 3$ intramolecular degrees of freedom, n being the number of atoms (or moieties) in the (finite) chain. This set may be specified directly in Cartesian space or generated as a function of internal parameters, such as bond lengths, bond angles, and dihedral angles, as is common in amorphous polymer glass simulations; the latter has been facilitated by the introduction of the generator matrix formalism of Flory.[26] In the case of polymer glasses, successive atom placements are generated stochastically, so that one cannot expect repetition in structure along the chain. One special feature of macromolecular crystals is the coupling between periodicity along the contour of the polymer chain and periodicity along the lattice dimension parallel to the chain propagation. In the case of ideal crystals the higher level order of the crystal implies translational periodicity along the chain and thus the formation of a rational helical conformation (one may consider rodlike and zigzag conformations to be degeneracies of the general helix description); to ensure periodicity, one employs a feature of the multichain ensemble, a lattice dimension, in describing the structure of the helix and hence the chain conformation. Previous simulations of ideal crystals have taken advantage of the periodicity characteristic of perfect crystals to generate additional transformations whose elements involve intermolecular distances and orientations derived from the dimensions, angles, and symmetries of the crystal lattice.[15,16] The result is a perfectly periodic ensemble created by replication in three dimensions of the minimum basis set of coordinates belonging to a single repeat unit of the rational helix. If one assumes only the existence of a "conformational repeat unit" (referred to hereafter as CRU), a substructure that is internally indistinguishable from any other along the chain contour in terms of conformation, the chain generation method satisfies the more general condition of helical periodicity. The special case of translational periodicity, or rational helicity, may be superposed by substituting a helix axis translation parameter for one of the internal degrees of freedom. In these cases, the number of intramolecular positional degrees of freedom reduces to $3N_{CRU} - 3$, where N_{CRU} is the number of atoms in the CRU. This repeat unit is typically taken to be one chemical repeat but could just as well be an integer multiple thereof. This number of internal degrees of freedom may be further reduced through the introduction of virtual bonds or other conformational constraints.

In the procedure developed here, we treat the polymer chain as a finite segment of the general coiling backbone polymer. Following Flory,[26] the Cartesian coordinate vector $\mathbf{X}$ for all atoms i in a single chain in the frame of reference of the first atom is generated:

$$\mathbf{X}_i^1 = \mathbf{L}_1 + \mathbf{T}_1\mathbf{L}_2 + \mathbf{T}_1\mathbf{T}_2\mathbf{L}_3 + \ldots + \mathbf{T}_1\mathbf{T}_2\ldots\mathbf{T}_{i-1}\mathbf{L}_i \quad (1)$$

$$\mathbf{L}_i = [l_i \quad 0 \quad 0] \quad (2)$$

$$\mathbf{T}_i = \begin{bmatrix} \cos(\vartheta_i) & \sin(\vartheta_i) & 0 \\ \sin(\vartheta_i)\cos(\phi_i) & -\cos(\vartheta_i)\cos(\phi_i) & \sin(\phi_i) \\ \sin(\vartheta_i)\sin(\phi_i) & -\cos(\vartheta_i)\sin(\phi_i) & -\cos(\phi_i) \end{bmatrix} \quad (3)$$

l_i, ϑ_i, and ϕ_i are the bond length, bond angle complement, and dihedral angle locating atom i in the frame of reference of atom $i - 1$. In this convention, $\phi_i = 0$ corresponds to the trans dihedral conformation. This may be accomplished by using the generator matrix $\mathbf{A}$:

$$\mathbf{X}_i^1 = \mathbf{A}_{[1}\mathbf{A}_2\mathbf{A}_3\mathbf{A}_4\ldots\mathbf{A}_{i-1}\mathbf{A}_{i]}, \quad i > 1 \quad (4)$$

$$\mathbf{A}_j = \begin{bmatrix} \mathbf{T}_j & \mathbf{L}_j \\ 0 & 1 \end{bmatrix} \quad 4 \times 4 \text{ matrix} \quad (5)$$

with

$$\mathbf{A}_{[1} = [\mathbf{T}_1 \quad \mathbf{L}_1] \quad 3 \times 4 \quad \text{matrix} \quad (6)$$

and

$$\mathbf{A}_{i]} = \begin{bmatrix} \mathbf{L}_i \\ 1 \end{bmatrix} \quad 4 \times 1 \text{ matrix} \quad (7)$$

In highly ordered polymer structures, it is appropriate to limit the set of unique conformational parameters to those of the CRU. The helical superstructure may be defined in terms of the translation along the helix axis (pitch, d_h), the directional rotation (twist, Θ_h) between identical points in successive structural units, and the radius (ρ_h), the distance from the axis to a reference point on the chain. The nonuniform helix is considered to be a perturbation of the uniform conformation. In order to capture local perturbations in helical structure, this model allows continuous variation of chain conformation during energy minimization through nonrational as well as rational helix conformations and includes the special cases of zigzag and extended-chain conformations. For the fully extended (i.e., zero helix twist) conformation it is necessary to introduce a switch from true helix representation and alignment to an approximation based on alignment of the major axis of the radius of gyration of the finite chain segment, in order to overcome the singularity in helix radius and consequent alignment problem that occur in the helix treatment. These calculations are presented in greater detail in the Appendix. Imperfect helix alignment, rigorously interpreted, creates the possibility for steric

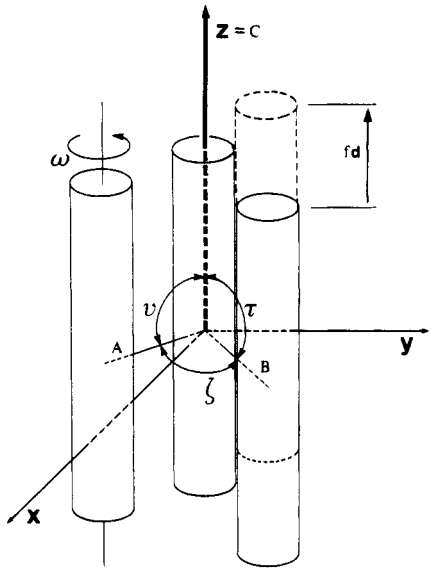

Figure 1. Definition of chain packing parameters.

interference between neighboring chains at points remote from the region explicitly described in the model. In allowing imperfect alignment of neighboring helices within the dominant explicit representation, one must ensure that the deviation from alignment be quantifiably small over large distances; that is, either (a) minor, low-energy torsional corrections (e.g., discommensurations) spaced at large intervals along the chain are capable of "periodically realigning" the set of chain propagation vectors or (b) the correlation lengths of the "crystallites" are sufficiently small relative to the alignment deviation to preclude any significant remote steric interferences. The first condition may be allowed through minor torsions which produce changes in chain alignment but which are energetically insignificant (e.g., an amide torsion of only 1° out of plane requires <0.05 kcal/mol but may alter the backbone contour vector by 2° and can create a local helix twist displacement of approximately 10°); the second condition may be deduced from the minimum dimension at which energetically significant steric overlap occurs.

Multichain Packing. The multichain structure is created through successive independent molecular coordinate generation accompanied by alignment of the primary chain axes. Again, the problem may be computationally simplified by assuming that individual chains are conformationally indistinguishable, analogous to the CRU assumption. In this case structure generation reduces to replication and reorientation of the parent chain conformation at points on a two-dimensional field. In a "disordered lattice", each neighboring chain may be located by a set of independent parameters describing orientation and translation of that chain from the "parent" position. In the paracrystalline structure, the vectors joining points in the "net" vary in magnitude and direction according to an a priori statistical probability. One may further limit the degrees of freedom by requiring correlation between the orientation of chains located at regular points in the net. In the perfect crystal, the net simplifies to a regular grid of translationally periodic points with only one or two characteristic orientations describing the setting of the chain at each of the grid points.

In these calculations, we employ the single conformation and periodic grid assumptions. The primitive cell parallelepiped has edge vectors **A**, **B**, and **C** and angles $\angle\mathbf{AB} = \zeta$, $\angle\mathbf{AC} = \nu$, and $\angle\mathbf{BC} = \tau$. Figure 1 illustrates this description of the crystal. We define the translation lengths, A and B, and the angles, ζ, ν, and τ, that orient the point net with respect to the major chain propagation axis **C**, chosen to coincide with the z-coordinate axis; the **A** vector is arbitrarily chosen to lie in the xz plane of the parent frame of reference. Chains are located at $m\mathbf{A} + n\mathbf{B}$, m and n being positive or negative integers. Each of the N_c *independent* chains may be oriented about its center of mass through the use of appropriate Euler angles, and $N_c - 1$ chains may be translated (relative to the parent chain) along their axes. From this selection of A, B, τ, ν, and ζ, it follows that, in Cartesian coordinates

$$\mathbf{A} = \begin{bmatrix} A\cos(90° - \nu) \\ 0 \\ A\sin(90° - \nu) \end{bmatrix}$$

$$\mathbf{B} = \begin{bmatrix} B\cos(90° - \tau)\cos\zeta' \\ B\cos(90° - \tau)\sin\zeta' \\ B\sin(90° - \tau) \end{bmatrix} \tag{8}$$

where

$$\cos\zeta' = (\cos\zeta - \cos\tau\cos\nu)/(\sin\tau\sin\nu)$$

The calculation of individual atomic coordinates for each atom i in chain j (which is located at $\mathbf{R}_j = m_j\mathbf{A} + n_j\mathbf{B}$ in the frame of the "parent") is accomplished by

$$\begin{bmatrix} \mathbf{X}_{ij} \\ 1 \end{bmatrix} = \begin{bmatrix} \mathbf{W}_j & \mathbf{R}_j \\ \mathbf{0} & 1 \end{bmatrix}\begin{bmatrix} \mathbf{X}_{i,1} \\ 1 \end{bmatrix} + f_j d\begin{bmatrix} \mathbf{W}_j & \mathbf{0} \\ \mathbf{0} & 1 \end{bmatrix}\begin{bmatrix} 0 \\ 0 \\ 1 \\ 0 \end{bmatrix} \tag{9}$$

$$\mathbf{W}_j = \begin{bmatrix} \cos\chi_j\cos\psi_j\cos\omega_j - \sin\chi_j\sin\omega_j & -\cos\chi_j\cos\psi_j\sin\omega_j - \sin\chi_j\cos\omega_j & -\cos\chi_j\sin\psi_j \\ \sin\chi_j\cos\psi_j\cos\omega_j + \cos\chi_j\sin\omega_j & -\sin\chi_j\cos\psi_j\sin\omega_j + \cos\chi_j\cos\omega_j & -\sin\chi_j\sin\psi_j \\ \sin\psi_j\cos\omega_j & -\sin\psi_j\sin\omega_j & \cos\psi_j \end{bmatrix} \tag{10}$$

d is the helix translation per structural repeat length (pitch), f_j is the translation, expressed as a fraction of the pitch, of chain j along its axis, and χ_j, Ψ_j, and ω_j are the Euler angles for placement of the jth chain. For the crystalline case, A, B, τ, ν, and ζ are constant, while in the paracrystal these may vary. While the $\mathbf{W}_j$ matrix is formulated generally above, in long-chain polymers Ψ_j is limited to values near 0 and 180° due to constraints on helix alignment. Chains that are mirror images of the parent are handled through multiplication of $\mathbf{W}_j$ with an inversion matrix. Under these conditions, helix translation along its axis may be sufficiently considered by $-0.5 < f_j < +0.5$. With the introduction of the regular point net the number of intermolecular degrees of freedom becomes $4N_c + 4$, while further simplification via $\chi_j = 0$ and $\Psi_j = 0$ yields $2N_c + 4$ degrees of freedom.

Energy Representation. Explicit Description. In order to calculate the potential energy for a representative crystal form, this method first assumes pairwise additivity of effective intermolecular interactions. The completely general description of the total potential energy for a construction consisting of L polymer chains may be

represented as

$$E^{\text{expl}} = \sum_{\substack{\text{all chains} \\ l}} E_l^{\text{intra}} + {}^1/_2 \sum_{\substack{\text{all chains} \\ l}} \sum_{\substack{\text{all chains} \\ l' \neq l}} E_{l,l'}^{\text{inter}} \quad (11)$$

l and l' refer to each of the L chains in the structure. Under the simplifying assumptions of structural repetition within and between chains, the average potential energy per structural repeat unit for a construction may be calculated explicitly as

$$E^{\text{unit}} = E^{\text{expl}}/LN_r \quad (12)$$

$$= (1/N_cN_r)\left[\sum_{m=1}^{N_c} E_m^{\text{intra}} + {}^1/_2 \sum_{m=1}^{N_c} \sum_{\substack{l=1 \\ l \neq m}}^{L} E_{m,l}^{\text{inter}}\right] \quad (13)$$

m refers to each of the N_c chains in the structure that is not related by a symmetry operation. The first term represents the total of the intramolecular interactions. For a single chain of h helix units, each consisting of k interacting atoms, the intramolecular energy may be calculated as

$$E^{\text{intra}} = \sum_{i=1}^{k} \sum_{j=1}^{hk} E(i,j) \quad (14)$$

where $E(i,j)$ is the general form describing the interaction between two atoms i and j. The second term in eq 13 represents the intermolecular potential energy. For two conformationally identical, parallel, interacting chains involving only distance-dependent interactions, one may take advantage of the nondirectional nature of spherically symmetric interactions to obtain the complete potential energy description from a reduced set of coordinates; this is employed only as an expedient to keep the memory requirements of the program to a minimum. For two interacting chains m and l, each of h helical repeat units consisting of k interacting atoms per helical repeat, the interaction energy may be calculated as (where i_m refers to the ith atom of chain m)

in general

$$E^{\text{inter}} = \sum_{i=hk/2}^{(hk/2)+k} \sum_{j=1}^{hk} E(j_l,i_m) \quad (15)$$

special case for parallel helices:

$$E_{l,m}^{\text{inter}} = \sum_{i=1}^{k} \sum_{j=1}^{hk} E(j_l,i_m) + \sum_{i=k+1}^{hk} \sum_{j=1}^{k} E(j_l,i_m) \quad (16)$$

Lattice Summation. While the above equations apply generally to multibodied systems, crystalline solids are most often idealized as perfectly periodic structures in three dimensions. This simplification precludes the representation of defects such as dislocations or discommensurations. However, it allows one to expedite the calculation of pairwise interactions through the use of lattice summations in three dimensions. A similar summation was employed by Anand[27] in arriving at an analytical equation for the cohesive energy of the infinite crystal in the absence of electrostatic forces. The simplification is conceptually identical with a numerical approximation of the Madelung constant for each new simulation. The translationally periodic infinite solid in three dimensions may be viewed as a construction consisting of unit cells displaced from a "parent" by an integer multiple of its edge vectors, where the only unique pairwise interactions that must be considered are those between the atoms making up one helical repeat unit of the parent chain and those of one helical repeat unit in each of the neighboring independent chains (i.e., those chains not displaced from the parent by a symmetry operation). The distance-dependent interaction may then be computed for an arbitrarily large construction through the use of a lattice summation:

$$E^{\text{lattice}} = (N_{\text{CRU}}/N_i) \sum_{n=1}^{N_p} \sum_{i=1}^{N_i} \sum_{j=1}^{N_i} A_{ij,n} \sum_{\text{L}} V_n(d_{ij}) \quad (17)$$

where i and j refer to the N_i interacting atoms that are crystallographically unique (i.e., belonging to the N_c independent chains). Thus if $N_c = 1$, N_i is equal to k, the number of atoms comprising one period of the helix. In general, $N_i = kN_c$. The premultiplier ensures that E^{unit} and E^{lattice} are calculated on the same basis. V_n is the distance-dependent potential function (e.g., d_{ij}^{-1}, d_{ij}^{-6}, or d_{ij}^{-12}) having multiplier $A_{ij,n}$ for atoms i and j; $\sum A_{ij,n}V_n(d_{ij})$ is the potential energy of interaction between a pair of atoms i and j (summation over n implied). The summation over the distance-dependent function in eq 17, $\sum_{\text{L}} V_n(d_{ij})$, is the lattice sum:

$$\sum_{\text{L}} V_n(d_{ij}) = \sum_{\lambda_a} \sum_{\lambda_b} \sum_{\lambda_c} V_n([\mathbf{d}^{\text{T}}_{ij,abc}\mathbf{d}_{ij,abc}]^{1/2}) \quad (18)$$

$$\mathbf{d}_{ij,abc} = \mathbf{d}_j - \mathbf{d}_i + \lambda_a\mathbf{A} + \lambda_b\mathbf{B} + \lambda_c\mathbf{C} \quad (19)$$

$\mathbf{d}_i$ is the location vector of atom i. $\mathbf{A}$, $\mathbf{B}$, and $\mathbf{C}$ are, again, the parallelepiped edge vectors; the summation coefficients λ_a, λ_b, and λ_c are selected large enough to effectively capture all significant interactions. Values of λ_a, λ_b, and λ_c up to 20 ($\approx$100 Å for most organic crystals) have been explored in this work, but, in general, truncation of λ_a, λ_b, and λ_c at values between 4 and 8 (depending upon geometry and potential energy description) was found to be adequate to approximate the energy of the infinite lattice to within 0.1 kcal/mol. This is in agreement with the findings of Tripathy et al.,[14] who concluded that the inclusion of a next-nearest-neighbor shell in the simulation of poly(vinylidene fluoride) was required to accurately estimate stabilization energy but that the inclusion of additional shells was unnecessary.

The above equations may be rewritten for helical periodicity as a summation over only the atoms of the helical subunits of each crystallographically unique chain. Then eq 17 holds, with N_i being the number of interacting centers in the helical subunit. The lattice sum becomes

$$\sum_{\text{L}} V_n(d_{ij}) = \sum_{a} \sum_{b} \sum_{s} V_n([\mathbf{d}^{\text{T}}_{ij,abs}\mathbf{d}_{ij,abs}]^{1/2}) \quad (20)$$

$$\mathbf{d}_{ij,abs} = \hat{\mathbf{W}}_s(\mathbf{d}_j - \mathbf{d}_{ij}^{\Delta}) + \mathbf{d}_{ij}^{\Delta} - \mathbf{d}_i + \lambda_a\mathbf{A} + \lambda_b\mathbf{B} + s\mathbf{F} \quad (21)$$

$$\mathbf{F} = [0 \quad 0 \quad d_h] \quad (22)$$

$$\hat{\mathbf{W}}_s = \begin{bmatrix} \cos(s\Theta_h) & -\sin(s\Theta_h) & 0 \\ \sin(s\Theta_h) & \cos(s\Theta_h) & 0 \\ 0 & 0 & 1 \end{bmatrix} \quad (23)$$

In eq 21, $\mathbf{d}_{ij}^{\Delta}$ is the vector describing the displacement of a point on the axis of the helix containing atom j from that on the axis of the helix containing atom i. (For example, $\mathbf{d}_{ij}^{\Delta}$ is equal to the chain placement vector $\mathbf{R}_j$ for summations involving the parent chain located at the origin of the Cartesian system.) The latter representation, while more computationally demanding than the case of translational periodicity in three dimensions, has the advantage

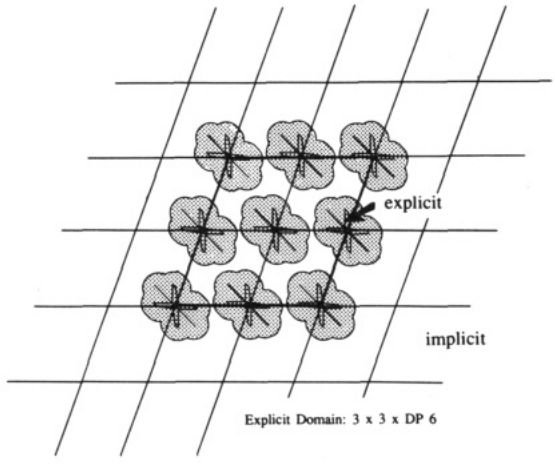

Figure 2. Representation of the packing structure as a local domain, described explicitly in terms of mutable atomic positions, embedded within an implicit perfect crystal.

that it can simulate incommensurate helices throughout the lattice. However, time trials using code optimized for concurrency on an Alliant FX/80 superminicomputer resulted in roughly an eightfold increase in CPU time for the helical periodicity representation. Under the special condition of helix commensuration (i.e., $\mathbf{C} = n\mathbf{d}$, $s = nc$, and $n\Theta_h = m360°$, m and n being integers), eq 21 reduces to the form of eq 19.

In our calculations we have retained the explicit potential energy calculation (eq 13) within a central "core" region consisting of the reference chain segment and its nearest-neighbor shell (3 × 3 × DP6: an array of chain segments three chains on a side, each segment possessing six monomer units) or in some cases the next-nearest-neighbor shell (5 × 5 × DP10). This region contains the dominant energy contributions which define the geometry of the structure. The explicit calculation allows one to represent local inhomogeneities such as defects in chemical constitution or tacticity or helix discommensuration and accounts for over 90% of the total calculated energy (98% in the 5 × 5 × DP10 case). The lattice summation calculates the contribution to the system energy of interactions with the surroundings, which ensures an accurate estimate of densification and the total cohesive energy of the condensed-phase structure. Thus the total energy to be minimized consists of both an explicit energy per unit contribution within a central parallelepiped and a lattice summation contribution for points outside of this parallelepiped:

$$E^{tot} = E^{unit}(K \times K \text{ array}, N_r \text{ repeat units}) + E^{lattice}(|\lambda_a|,|\lambda_b| > K/2, |\lambda_c| > N_r/2) \quad (24)$$

The resulting picture, illustrated in Figure 2, may be viewed as a potentially imperfect pseudocrystalline parallelepiped embedded within a defect-free crystalline universe. In this manner the model attempts to capture both geometry and energy features of pseudocrystalline solid structures.

Force Field. The choice of a potential energy force field depends upon the molecular architecture. The potential energy summation must converge as its range is extended over successive interaction shells. Akin to earlier work described in the literature,[15,28,29] this model uses a modified valence force field (VFF) description for bonded two- and three-atom deformations and empirical torsional energy functions for bonded four-atom deformations. Nonbonded interactions are represented by a modified 12–6–1 Lennard-Jones/Coulomb energy function:

$$E_{ij} = A_{ij,12}/d_{ij}^{12} + A_{ij,6}/d_{ij}^{6} + A_{ij,1}/D(d_{ij}) \quad (25)$$

where

$$A_{ij,12} = 0.5A_{ij,6}(r_i + r_j)^6 \quad (26)$$

$$A_{ij,6} = -(\epsilon_i\epsilon_j)^{1/2}(r_i + r_j)^6 \quad (27)$$

$$A_{ij,1} = q_iq_j/4\pi\epsilon_0 \quad (28)$$

$$D(d_{ij}) = 1; \quad d_{ij} < d^*$$
$$= D_B \exp(-\kappa/d_{ij}); \quad d_{ij} > d^* \quad (29)$$

$$\kappa = \ln (D_B)d^* \quad (30)$$

i and j refer to the atoms separated by the distance d_{ij}; ϵ and r are atom contributions to the van der Waals potential energy well depth and location, respectively, and the q are partial atomic charges, which may be derived from data on low molecular weight compounds or estimated by well-established quantum mechanical methods. ϵ_0 refers to the vacuum permittivity. A distance-dependent dielectric constant has been employed, using the approximation of Block and Walker[30] to reflect the different dielectric environments experienced by short- and long-range charge interactions. At short distances, the effective dielectric constant is unity; at larger distances, it asymptotically approaches its static bulk value, D_B. The constant κ is chosen to ensure convergence of the two portions of the dielectric function at the crossover distance d^*. A quintic spline in D between $1.0 < d_{ij}/d^* < 1.1$ is used to join the regions smoothly. A similar attenuation was employed with good results in the modeling of a polar polymer glass.[31] It is readily demonstrated that interactions of higher than third order in inverse distance (e.g., the sixth-order and twelfth-order induction/dispersion terms) are convergent as interaction distances become infinite; such is not necessarily the case of the first-order electrostatic term. To ensure convergence of the summation over the electrostatic interactions, one requires that the structure be electrically neutral. Secondly, it is necessary in this method that the characteristic crossover distance d^* be constant for all atoms in the structure, in order to ensure that there is no net accumulation of residual electrostatic interaction as an artifact of the boundary between explicit energy calculation and lattice summation.

III. Application to Poly(*p*-phenyleneterephthalamide)

This model was developed primarily with an interest in the particular features of highly extended, stiff-chain polymers such as the wholly aromatic polyamides, polyesters, and other conformationally restricted long-chain polymers. This family of materials has attracted considerable interest for the characteristically high temperature stabilities and tensile moduli of its members.[32,33] In the solid state, these materials are characterized by a high degree of molecular alignment. However, as a result of their relative inflexibility, they do not exhibit the conventional crystalline domain/amorphous domain segregation typical of more flexible polymers, as evidenced by the lack of an amorphous halo in X-ray diffraction measurement.[34] Instead, the solid-state structures tend to arrange into condensed-phase nematic arrays. Aramid fibers specifically exhibit evidence of paracrystalline distortions of the second kind along the chain alignment axis. For purposes of developing and testing the model we directed out attention to the in-depth analysis of poly(*p*-phenyleneterephthalamide) (PPTA). This structure

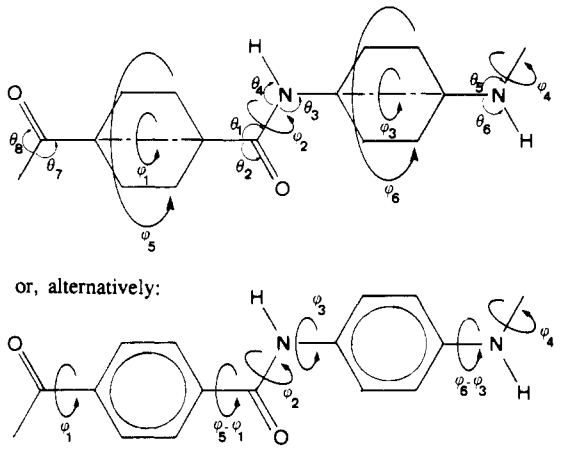

Figure 3. A segment of poly(*p*-phenyleneterephthalamide) (PPTA) with all torsion angles in their zero positions.

possesses several features which recommend it for our purposes. First, PPTA has been discussed extensively in the literature and is the only such rigid-rod polyamide for which there exists a sufficient set of experimental data, encompassing crystallographic and macromorphological descriptions, thermomechanical behavior, solution behavior, radiation absorption, and response to chemical exposure. Second, at least two crystal polymorphs have been reported experimentally, and numerous references to additional crystalline or paracrystalline forms have been made.[28,35-38] Third, PPTA is readily available, in the form of Du Pont's Kevlar fiber, for additional processing and testing against model predictions.

Even on a stand-alone basis, PPTA possesses several features of particular interest for molecular analysis. (1) This polymer consists entirely of alternating para-linked phenylene rings and amide linkages; each of these rigid moieties is a polyatomic group which acts in a concerted manner. The phenylene moiety may rotate without significant effect on the helical chain conformation, but with possibly major impact on chain packing. (2) The amide moiety is known to form intermolecular hydrogen bonds between proximate hydrogens and oxygens. (3) There is the possibility for further energetically favorable interactions due to π-bond overlap between adjacent phenylene and amide moieties within a chain or between proximate phenylene moieties between chains. These features create a vastly different environment from the neutral, flexible-chain aliphatics addressed by other investigators. New problems of both intramolecular description and intermolecular behaviors must be addressed in order to produce a meaningful picture by atomistic modeling.

Chain Description. The polymer chain is described as an ensemble in Cartesian space of its constituent atoms, all of which are expressed explicitly. The repeat unit of the polymer chain is illustrated in Figure 3. All atoms in the chain are treated as point centers of force for calculation of interaction energies. We hold all bond lengths and bond angles constant, with the exception of the eight "backbone" angles (labelled ϑ_1 through ϑ_8 in Figure 3); during the course of this work, we discovered that the optimization trajectory was considerably improved when these crucial angles were allowed to change during ring rotation. The phenylene rings are represented as rigid, hexagonal constructions of the ten bonded constituent atoms. The bonding at the trivalent amide carbons and nitrogens in the amide group is fixed in the planar sp^2 hybridization configuration. In this way the number of internal degrees of freedom was reduced from eighty-four to fourteen: the

Table I
Fixed Bond Lengths and Valence Force Field (VFF) Constants for Variable Backbone Angles

angle[a,b]	k_i, kcal/deg^2	bond	l, Å
CC_OO (ϑ_2)	0.088	C_{ar}–C_{ar}	1.40
CC_ON (ϑ_1, ϑ_7)	0.088	C_{ar}–H	1.10
C_ONH (ϑ_4)	0.050	C_{ar}–C_{am}	1.50
C_ONC (ϑ_3, ϑ_5)	0.088	C_{ar}–N	1.41
CNH (ϑ_6)	0.050	C_{am}=O	1.24
NC_OO (ϑ_8)	0.088	C_{am}–N	1.39
		N–H	1.00

[a] Angle bending energy = $k_i(\vartheta_i - \vartheta_0)^2$ where $\vartheta_0 = 120°$ in all cases. [b] C_O is the sp^2-carbonyl carbon atom.

eight bond angles and six torsion angles (ϕ^1 through ϕ_6 in Figure 3) of the structural unit. ϕ_1 and ϕ_3 represent torsions about the virtual bonds spanning the rigid phenylene moieties, while ϕ_2 and ϕ_4 represent torsions about the C–N bond of the amide moiety; these four torsions influence the helical structure of the chain directly. ϕ_5 and ϕ_6 represent rotations of the ring planes about the C1–C4 axes, independent of the larger helical structure of the chain.

Parameterization of the Force Field. A simple VFF description was employed for the eight bond angles, using values taken from Tashiro et al.[28] Table I gives the important parameters for the VFF description, along with all the bond lengths and bond angles required. Parameterization of the 12–6–1 nonbonded interatomic potential energy function for the amide moiety has been taken directly from the work of Lifson and co-workers on the development of a self-consistent force field encompassing low molecular weight alkane, alkene, amide, and carboxylic acid crystals;[39-42] this force field has been designed to reproduce hydrogen-bonding interactions implicitly. For the carbons and hydrogens of the aromatic rings, we initially attempted to use the values suggested by Lifson and co-workers for aliphatic carbons and hydrogens, as has been done previously by others.[8,43] The van der Waals radii for the aromatic carbons were eventually reduced by 10% from the aliphatic carbon values suggested by these investigators, in order to improve the torsional energy approximation for ring rotation (see below). We deem this slight correction to be minor in light of the margin of error inherent in such estimates of van der Waals radii.

The partial atomic charges required for the atom-centered electrostatic interactions involving phenylene ring atoms, however, are not generally available. To estimate these, it was necessary to embark upon a series of calculations using various semiempirical quantum mechanics packages for a homologous series of low molecular weight aromatic amides. In each case, molecules in the series were completely optimized with respect to bond lengths, bond angles, and bond torsions, subject to the restriction of planar hexagonal phenylene rings, in accord with the model description. Results for the members of the series were compared for internal consistency of geometry and charge distribution. Where possible, individual members were checked for agreement with available experimental data for ring torsions and nonzero electrostatic moments. A description of the estimation procedure is available in greater detail elsewhere.[44] The final atomic charges were chosen to reproduce dipole and quadrupole data through assignment of partial charges located at the atom centers and to ensure local charge neutrality in the amide N–H, the amide C=O, and the phenylene ring. The calculated charges on the atoms of the amide group are comparable to those proposed independently by Hagler et al.[41] and used in conjunction

Table II
6-12 Nonbonded Atomic Potential Parameters and Elementary Charges Used in the Electrostatic Potential

atom	ϵ, kcal/mol	r, Å	q,[a] elementary charge
C(phenylene, 1 and 4)	0.039	1.96	−0.06
C(phenylene, 2 and 3)	0.039	1.96	−0.12
H(phenylene)	0.038	1.37	+0.14
C(amide)	0.147	2.03	+0.38
H(amide)	0.0	0.0	+0.28
N	0.169	1.96	−0.28
O	0.232	1.60	−0.38

[a] The value for the bulk dielectric constant D_B was 3.5, and the Block-Walker crossover distance d^* was 3.3 Å.

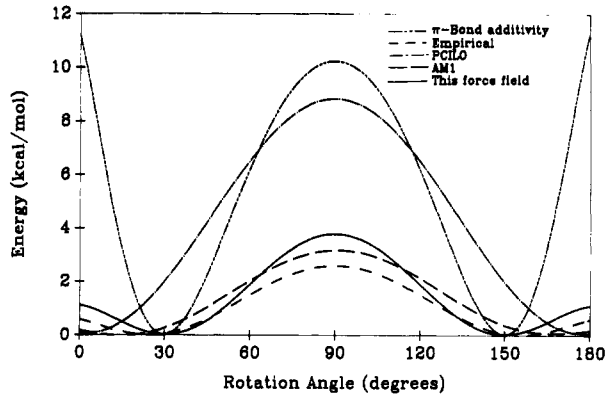

Figure 4. Rotation energy functions suggested for the phenylene ring connected to the amide nitrogen in benzanilide: (a) π-bond additivity;[28] (b) empirical fit;[43] (c) PCILO calculation;[45] (d) AM1 calculation (this work); (e) composite force field (this work).

with their induction/dispersion parameters; the latter were retained in our work for purposes of consistency. Partial atomic charges and nonbonded potential energy parameters used in this work are listed in Table II.

For the C–N amide torsion, we have used the potential energy function of Jorgensen and Swensen,[10] derived from NMR data on *N*-methylacetamide. The interaction between the adjacent ring and amide moieties prefers coplanarity of the bond planes of these two groups in order to effect the delocalization of electrons in π-bond orbitals; however, this coplanarity is precluded by steric overlap between the hydrogens on the ring and the pendant atoms (O and H) on the amide group. Numerous (disparate) estimates for the phenylene–amide correlated torsion energy have been reported, indicating the general lack of consistent quantitative information on this type of distributed interaction. Estimates have originated from semiempirical quantum mechanics calculations,[45] π-bond group additivity considerations,[28] and empirical fitting to experimental crystal data for low molecular weight analogues.[43] We have further explored this torsion using AM1[46] semiempirical quantum mechanics calculations, as described in greater detail elsewhere.[44] Figure 4 shows several energy functions reported in the literature, along with AM1 results for the rotation of the phenylene ring connected to the amide nitrogen in benzanilide. Figure 5 shows similar predictions, including AM1 rotation results for the ring connected to the amide carbon in benzanilide. For parameterization purposes, we have employed two-parameter cycloidic torsion energy functions which, in combination with the nonbonded atomic interactions, are consistent with the available torsional energy estimates. These, along with the amide torsional energy function of Jorgensen and Swensen, are reproduced below, with parameters presented in Table III. Because the nonbonded interactions are retained explicitly for interactions between atoms in the ring and the amide group, the

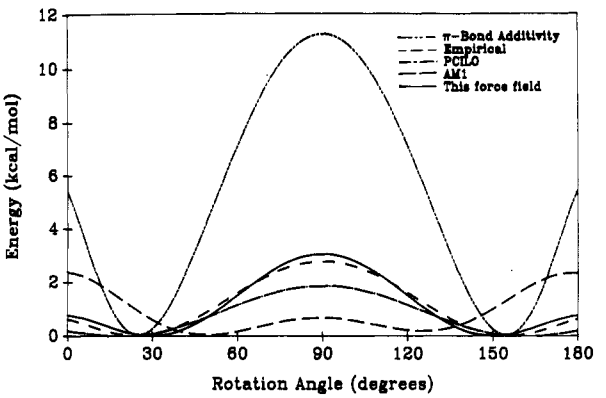

Figure 5. Rotation energy functions suggested for the phenylene ring connected to the amide carbon in benzanilide: (a) π-bond additivity;[28] (b) empirical fit;[43] (c) PCILO calculation;[45] (d) AM1 calculation (this work); (e) composite force field (this work).

Table III
Intrinsic Torsional Energy Function Parameters[a]

torsion	$V_{a,1}$[b]	$V_{a,2}$[b]	V_d[b]	m_d
amide (ϕ_2, ϕ_4)	2.8	21.2		
diacid ring (ϕ_5, $\phi_5 - \phi_1$)			9.0	0.2
diamide ring (ϕ_6, $\phi_6 - \phi_3$)			13.0	0.4

[a] See text for details, eqs 31–33. [b] All values in kcal/mol.

torsional potentials describing ring rotation may be attributed to the phenomenon of electron distribution between the two moieties.

$$E^{\text{tor,amide}} = {}^1/_2V_{a,1}(1 - \cos\phi_2) + {}^1/_2V_{a,2}(1 - \cos 2\phi_2) \quad [\text{same for } \phi_4] \tag{31}$$

$$E^{\text{del,phenylene–C=O}} = {}^1/_2V_d(1 + \cos(y)) \tag{32}$$

$$\phi_5 = {}^1/_2(y - m_d \sin(y)) + \pi \quad [\text{same for } (\phi_5 - \phi_1)]$$

$$E^{\text{del,phenylene–N–H}} = {}^1/_2V_d(1 - \cos(z)) \tag{33}$$

$$\phi_6 = {}^1/_2(z - m_d \sin(z)) \quad [\text{same for } (\phi_6 - \phi_3)]$$

Simulation Procedure. The approach to structure optimization plays a major role in the validity of model predictions. Time and computational constraints limit the thoroughness of any such general investigation. Approaches to analysis by simulation may, however, be classified according to the goals they seek to achieve. Where one is interested primarily in elucidation of a known structure or defined region of parameter space or in comparisons between such predefined domains, it is possible to take advantage of previous (e.g., experimental) information to limit the range of investigation, making it relatively straightforward to identify minima of immediate interest and to establish the nature of the local parameter space. This solution contains no assertions about the global nature of the minima thus identified and may depend strongly upon the choice of a starting point. Where one is concerned with a first-principles approach to materials investigation or where experimental data are not available, it becomes necessary not only to locate minima but to establish confidence in their global relation. Unfortunately, this may only be assured by investigating the whole of parameter space and identification of all minima therein, a time-intensive process whose end cannot be a priori guaranteed. The latter problem necessitates an initial grid scan of parameter space, with a decision criterion established to identify relevant regions of the

Table IV
Starting Point Mesh Used in Multichain Search Minimization

parameter	range	step size
interchain distance, Å	4.5–9.0	2.25
interaxial angle, deg	30–90	20
chain placement angle, deg	0–360	20
chain translation[a]	−0.5 to +0.5	0.25

[a] Chain translation is expressed as a fraction of the helix translation distance; values outside of this range are redundant with respect to rotation/translation operations.

parameter field for further analysis. This approach, of course, suffers from grid density dependencies and response of the minimization algorithm to the convolution of the multivariate phase space.

Our analysis to identify likely structures for polymer packing proceeds according to the following strategy. As an initial approximation, we assume that chain conformation and chain-packing considerations may be decoupled and considered independently. This is the most common approach taken in molecular mechanics and X-ray structure factor fitting procedures and, as was mentioned previously, is where most previous efforts have stopped. As a result of this approximation, we may first employ single-chain simulations to identify those conformations which are of lowest energy and are most likely to meet packing density criteria. In addition, we are primarily interested in the highly oriented structures produced during fiber spinning. Such elongational processing steps are known to favor the formation of extended-chain conformations prior to vitrification or crystallization and concurrent loss of conformational mobility. On the basis of this, we exclude conformations of low helical pitch from further consideration.

As a second step, we perform successive grid scans of the multivariate packing parameter space using fixed chain conformations at a predetermined packing density, initially without minimization of energy with respect to intermolecular packing parameters, starting with conformations of smallest helix diameter; we conclude the search with those conformations which are of sufficiently large helix diameter to preclude the realization of reasonable packing energies in the entire parameter space. In some cases, such scans are repeated with minimization of potential energy with respect to packing parameters. The grid density was chosen based on experience with the polymer in question and reflects a subjective trade-off between computation time and comprehensiveness. Table IV lists the starting point mesh parameters, ranges, and mesh densities employed in PPTA.

In the third step, we drop the approximation of independent intramolecular and intermolecular behaviors and concentrate on those areas of conformation/chain packing space that signal the location of low-energy local minima. The relevant domains thus identified are searched by means of nonlinear multivariate potential energy minimizations using an unconstrained Davidson–Fletcher–Powell quasi-Newton algorithm with "approximate Hessian" estimation.[47]

PPTA Simulation Results. Single Chain. To reduce the parameter space of relevance for chain-packing calculations, we first looked for the preferred conformation behavior of the isolated chain. For this purpose, we consider the PPTA chain as a string of torsion angle triplets, composed of the phenylene–C–N, amide, and C–N–phenylene torsions (ϕ_3, ϕ_2, and ϕ_1, respectively, in Figure 6), each triplet being identical and alternating in order along the chain due to the symmetry of the monomer

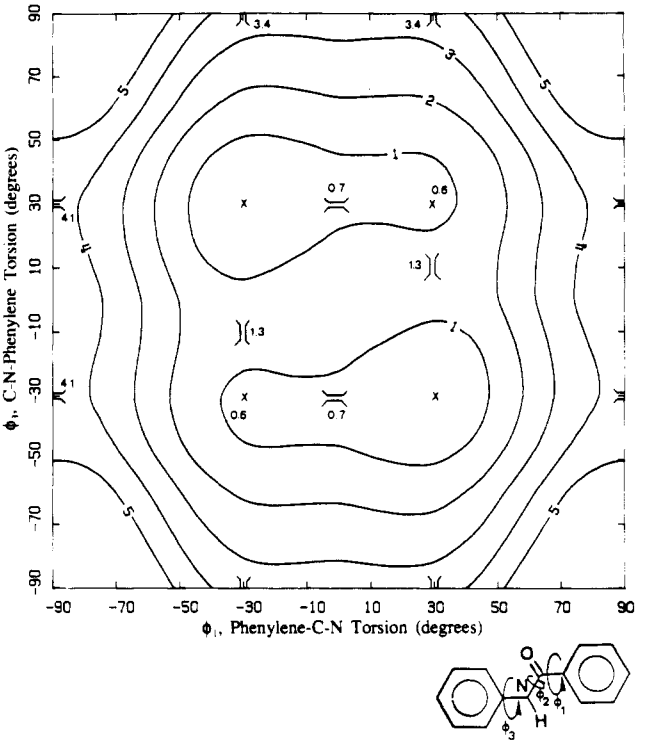

Figure 6. Potential energy contour for benzanilide as a function of the ring torsions ϕ_1 and ϕ_3. The symbol × denotes a local minimum in potential energy, while the symbol ⋈ denotes a saddle point. Contour levels are as indicated, in units of kcal/mol.

units. This simplification arises from the assumption that intramolecular interactions are essentially decoupled across the rigid phenylene moieties. Since the amide torsion exhibits a strong preference for the trans or cis conformation, it suffices to study the conformation energy as a function of ϕ_1 and ϕ_3, with ϕ_2 always assuming a position of minimum energy. Figure 6 shows such an energy contour map for benzanilide with the amide torsion optimized about its trans conformation; a similar map with minimization of the amide torsion about the cis conformation exhibits minima near [30°,150°] and [150°,30°], but these are energetically less favorable (by 4–5 kcal/mol of repeat units) compared to the trans amide conformation. Of the possible monomer conformations, only those of a highly extended character will pack to densities realized in the solid state for PPTA without unreasonable penalties in intermolecular energy. On the basis of this, we have concentrated on those conformations having rodlike or crankshaftlike conformations for chain-packing studies. Of these, only the all-trans rodlike conformations appear in the final list of lowest energy packed structures, as will be seen in the next section. This essential rigidity ensures that chain alignment plays a dominant role in packed structure formation.

Multiple Chains. A screening of the packing energy using the most probable conformations in a general grid assembly and minimizing simultaneously with respect to both intramolecular and intermolecular degrees of freedom indicates considerable correlation between chain orientations in the packed structures. This is demonstrated in Figure 7, where the concentration of packing minima along the diagonals of a plot of total potential energy versus chain setting angles ω (for a lattice composed of two independent chains initially in the all-trans conformation with successive phenylene rings oppositely rotated; ω is defined by the rotation of the first amide plane of the chain out of the AC plane of the parallelpiped, Figure 1)

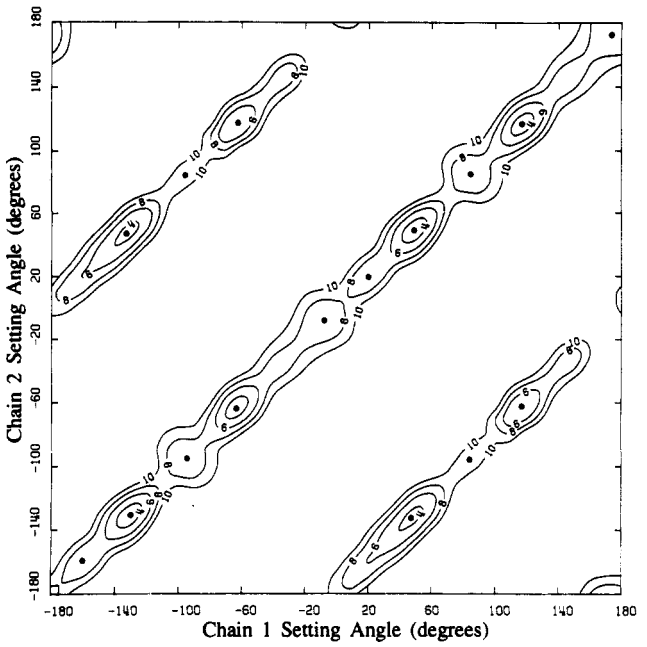

Figure 7. Energy contours for packing of extended conformations of two independently orientable chains of like conformation of PPTA as a function of the two setting angles ω_1 and ω_2. The symbol • denotes a local minimum in potential energy. Contour levels are as indicated, in units of kcal/mol of constitutional repeat units.

is indicative of the predominant formation of sheetlike structures in PPTA; similar maps were found for packing of chains in other initial conformations.

From such maps, those structures having the lowest total potential energy were identified as possible crystal structures. By means of the scan-and-search procedure, a listing of local minima is obtained; from this set, we discard as irrelevant those minima whose statistical significance, according to a Boltzmann-weighted probability of occurrence on a per repeat unit basis, falls below our cut-off criterion of 0.2, or 20% probability of occurrence.

The final analysis suggests up to eight distinct and viable crystalline polymorphs, all having cohesive energies within a variance of 6%, or a range of 2.4 kcal/mol (10 cal/g) between the highest and the lowest energies. Quantitative description is given in Table V. It may be noted that in the construction of this model we have intentionally favored a general parallelepiped description for chain packing, involving the vectors **A**, **B**, and **C**, over a presumed unit cell or superposition-of-unit cells description. There are also some minor quantitative differences between the parameters listed in Table V and those which may be deduced from Figure 7, due to refinements of the model and elimination of redundant structures prior to tabulation in Table V. For ease of clarification, we have converted the structural parameters in Table V from the generalized parallelepiped description to a parameter set more amenable to crystallographic interpretation and have reported parameters in both conventions. The appropriate unit cell descriptions were selected from the infinite number of possible descriptions based on a preference for interaxial angles $\alpha = \angle\mathbf{bc}$, $\beta = \angle\mathbf{ac}$, and $\gamma = \angle\mathbf{ab}$ closest to 90°. It may readily be seen that the crystallographic cell, described by the vectors **a**, **b**, and **c**, obeys the relations $\mathbf{c}||\mathbf{C}$ and $\mathbf{a} \times \mathbf{b}||\mathbf{A} \times \mathbf{B}$. Similarly, the chain setting angles are reported relative to the *bc* facet (the $\mathbf{b} \times \mathbf{c}$ plane), as was done by Northolt for PPTA, rather than relative to the arbitrarily selected $\mathbf{A} \times \mathbf{C}$ plane of the parallelepiped.

From this basis set of lowest energy packing minima, one may draw several conclusions concerning the preferred structure of PPTA:

(1) The backbone features of individual chain conformations are in reasonable agreement with those employed by Northolt in his crystal structure analysis. Table VI shows the final values of the important backbone angles and torsions of the chain conformation in the packed geometries. Angles of 10 ± 4° are formed between the phenylene rings and the chain propagation axis, and torsions about the amide bond vary from 2 to 7° and are generally balanced by alternate plus/minus torsions of equal magnitude in consecutive amide moieties. This conformation orients the amide dipoles in all cases in nearly antiparallel fashion as one travels along the chain axis. Phenylene ring positions about the C1–C4 axes relative to the plane of the adjacent amide bond show a preference for out-of-plane rotation (see Table VI), as expected from the isolated-chain energetics reported in the previous section and from reports in the literature.[28,34,43] Packing considerations do not appear to preclude either of the two possible directions of ring rotation. However, the chain packing does appear to have a considerable effect on the magnitude of out-of-plane rotation, with values ranging between roughly 15 and 43° for either ring.

(2) While no hydrogen-bonding potential energy function has been explicitly included, nevertheless the geometry and energy character of "hydrogen bonding" between amide groups in neighboring chains is reasonably reproduced. This is in good agreement with the findings of Hagler et al.[41] For the final eight structures, the average O···H "bond" distance is 2.3 Å, with an N–H···O angle of 160°. The interaction energy attributable to the hydrogen bond varies between 1.8 and 3.8 kcal/mol and is largely due to the strong electrostatic attraction between the hydrogen–oxygen pair. Hagler et al. suggest that their force field for the amide moiety, employed unchanged in this work, yields an optimum hydrogen-bonding distance of 2.1 Å and a "bond energy" of 2.4 kcal/mol; in their study of low molecular weight amide crystals, predicted hydrogen bond lengths were slightly lower, ranging from 1.9 up to 2.1 Å, with an N–H···O angle of 145–175°. Our calculated bond length of 2.3 Å lies intermediate between these values and the 2.9 Å proposed by Ladell and Post[48] to be typical for amide crystals. The 160° angle is essentially identical with that assumed by Schroeder and Lippincott[49] in their explicit potential function representation of the N–H···O hydrogen bond.

(3) The nature of the chain–chain interactions is consistent across the set of eight structures, as suggested by the orientation correlation maps, and determines the extent of lateral order (perpendicular to the chain axis) seen in the polymorphs. The hydrogen-bonding interactions for each chain lie roughly within a plane as a result of the chains' all-trans conformations; this leads to the association of chains by hydrogen bonding into sheets and allows one to distinguish between interchain energies within and between sheets. These energies may be broken down into their van der Waals and electrostatic components for each cell structure. Table VII shows the sources of interactions between two chains within the same sheet. In each polymorph, the dominant contribution (66–90% of the total) is electrostatic. Furthermore, the electrostatic component may be decomposed into amide–amide interactions and phenylene–phenylene interactions as shown, with the remainder being a cross contribution from amide–phenylene interactions; clearly, the electrostatic interaction is predominantly between amide moieties and is quite

Table V
Multichain Energy Minimization Results: Structural Parameters for the Eight Most Probable Unit Cells

structural parameter	structure ID 1	2	3	4	5	6	7	8
a, Å	6.8	7.1	8.3	8.4	8.4	8.5	8.4	4.8
b, Å	6.2	5.9	5.0	4.9	4.9	4.6	4.9	5.0
c, Å	13.2	13.1	13.1	13.1	13.1	13.1	13.1	13.1
α, deg	90	93	90	86	80	79	85	55
β, deg	90	92	90	78	89	94	93	95
γ, deg	88	92	92	89	90	93	90	96
chain locations (ab projection)	[0,0] [1/2,1/2]	[0,0] [1/2,1/2]	[0,0] [1/2,1/2]	[0,0] [1/2,1/2]	[0,0] [1/2,0]	[0,0] [1/2,0]	[0,0] [1/2,0]	[0,0]
chain setting angles relative to the bc facet, deg	6 −174	2 2	18 −161	12 13	−2 −1	−9 −9	2 1	2
intersheet translation, Å	6.2	6.6	5.9	6.6	2.4	3.1	6.6	2.7
helix twist Θ_h, deg	0	0	4	6	3	0	1	4
monomer phenylene ring rotation, deg								
diacid ring ϕ_5	−16	−30	−26	−35	−43	39	43	34
diamide ring ϕ_6	15	21	43	36	40	38	33	29
cohesive energy, kcal/mol of repeat units	40.5	38.5	38.3	38.2	38.1	39.3	39.7	39.6
density, g/cm^3	1.42	1.45	1.45	1.49	1.50	1.57	1.47	1.56
parallelpiped description								
A, Å	4.7	4.5	4.8	4.9	4.2	6.2	6.4	5.0
B, Å	4.6	4.7	4.9	4.8	6.4	4.4	4.2	4.8
C, Å	13.2	13.1	13.1	13.1	13.1	13.1	13.1	13.1
τ, deg	90	90	90	81	97	98	93	95
ν, deg	90	94	90	77	89	88	88	85
ζ, deg	85	81	62	61	50	48	50	96
ω_1, deg	127	128	101	110	92	146	138	92
ω_2, deg	−53	128	−79	110	92	146	138	92
f_2	0.47	0.50	0.45	0.50	0.18	−0.25	0.50	0.0

Table VI
Representative Chain Conformation Angles Realized in Packed Structures

angle	value, deg	torsion	value, deg
C_{ar}–C_{am}–N	118.7 ± 0.3	N–C_{am}–C_{am}–N	−2.7 ± 3.0
C_{ar}–C_{am}=O	120.4 ± 0.4	C_{am}–C_{am}–N–N	+4.7 ± 3.1
C_{am}–N–H	117.0 ● 1.8	C_{am}–N–N–C_{am}	−1.8 ± 1.6
C_{am}–N–C_{ar}	126.0 ± 3.3	N–N–C_{am}–C_{am}	−4.5 ± 2.7
C_{ar}–N–H	117.3 ± 1.6	diamide phenylene	15–43 o.o.p.[a]
C_{ar}–N–C_{am}	126.0 ± 3.0	diacid phenylene	16–43 o.o.p.[a]
N–C_{am}=O	120.5 ± 0.6		
N–C_{am}–C_{ar}	120.0 ± 1.0		

[a] o.o.p. refers to rotation out of the plane of the preceding amide group.

specific in nature. Thus one finds an interaction of considerable magnitude and moiety-to-moiety specificity between chains within a hydrogen-bonded sheet, which ensures axial register and consistent interchain separation distances. This interaction takes priority in organizing the packing of chains lateral to the axis of chain alignment in the solid state. Table VIII, on the other hand, illustrates the nonspecific nature of the interchain energetics between chains in neighboring sheets. Of particular interest is the magnitude of the total energy, which, contrary to previous conjecture, is comparable to that between chains within a sheet. However, the source of this interaction energy is evenly split between van der Waals and electrostatic contributions, and the latter in turn is relatively evenly split among the interactions between different moieties. From this one may conclude that while sheet–sheet separation is a high-energy process, sheet–sheet slip remains a viable deformation mode, and the lack of preferred register between sheets is largely responsible for the multiplicity of crystal forms witnessed in the model analysis. This tendency toward slip is consistent with compressive failure observations reported in the literature.[50,51]

(4) The predicted densities lie between 1.42 and 1.57 g/cm^3; these values result largely from the choice of 12–6–1 potential energy parameters. While the model does not explicitly consider thermal effects, the force field parameters implemented were derived from experimental data on low molecular weight amide crystals at 25 °C and therefore incorporate thermal motion effects into the force field parameters themselves. The resulting densities are in good agreement with reported PPTA solid densities of 1.45–1.50 g/cm^3.

(5) The cohesive energy is defined as the increase in internal energy per mole of a substance upon removal of all intermolecular forces.[52] This value is readily calculated as the difference between the energy of the packed structure and the energy of the isolated-chain conformation. The Hildebrandt solubility parameter may then be calculated as the square root of the cohesive energy density:

$$\delta = (E_{coh}/V)^{1/2} = (E_{coh}\rho/M_w) \tag{34}$$

In this manner, for the cohesive energy and corresponding solubility parameter for PPTA based on the set of eight packing structures we obtain (per mole of repeat units)

$$E_{coh} = 39.0 \pm 1 \text{ kcal/mol}$$

$$15.3 < \delta < 16.1 \text{ (cal/cm}^3\text{)}^{1/2}$$

or

$$31.2 \times 10^3 < \delta < 32.8 \times 10^3 \text{ (J/m}^3\text{)}^{1/2}$$

This range is quite reasonable in light of the relative insolubility and high-temperature melting behavior of PPTA. While experimental values for solubility parameters of aromatic polyamides are not available, values for some related aliphatic polyamides are 12.7 and 13.6 (cal/cm^3)$^{1/2}$ [or 25.9 × 10^3 and 27.7 × 10^3 (J/m^3)$^{1/2}$] for poly(8-aminocaprylic acid) and poly(hexamethylene adipamide), respectively;[52] we would expect the aromatic polyamide value to be somewhat higher, reflective of its reduced solubility in all but the most aggressive solvents.

Finally, significant differences between the eight final structures should be noted. All geometries except struc-

Table VII
Intermolecular Bonding Energy: Component Contributions to Chain–Chain Interaction *within* a Sheet (All Values in kcal/mol of Repeat Units)

	structure ID							
	1	2	3	4	5	6	7	8
total 12–6	2.1	2.6	2.8	2.2	2.6	1.4	2.5	0.9
total electrostatic	5.8	5.1	5.4	6.9	7.1	8.1	7.5	8.3
amide–amide electrostatic	3.8	3.3	3.5	5.7	5.9	7.4	5.7	6.8
phenylene–phenylene electrostatic	0.7	1.1	1.9	1.7	1.5	1.9	2.1	2.1
total	7.9	7.7	8.2	9.1	9.7	9.5	10.0	9.2

Table VIII
Intermolecular Bonding Energy: Component Contributions to Chain–Chain Interaction *between* Sheets (All Values in kcal/mol of Repeat Units)

	structure ID							
	1	2	3	4	5	6	7	8
total 12–6	4.4	3.8	3.2	3.4	4.4	4.3	4.5	4.6
total electrostatic	2.5	2.5	4.6	2.7	3.8	2.5	4.8	3.1
amide–amide electrostatic	0.8	1.1	1.7	1.2	0.8	0.3	1.7	0.2
phenylene–phenylene electrostatic	1.3	1.6	1.5	1.2	1.3	2.1	2.6	2.2
total	6.9	6.3	7.8	6.1	8.2	6.8	9.3	7.7

ture 8 contain two chains per unit cell. The chains in structures 1–4 all intersect the *ab* plane at [0,0] and [$^1/_2$,$^1/_2$]. Of these, structures 1 and 3 each contain conforma tions having oppositely rotated phenylene rings and sheet packing such that amide moieties in successive sheets are in register along the *c* dimension with alternating direction of the amide dipoles; structures 2 and 4 are the analogues, respectively, of structures 1 and 3, with the distinction being the codirection of amide dipoles in successive sheets. The chains in structures 5–7 intersect the *ab* plane at [0,0] and [$^1/_2$,0]. Only structure 5 has the adjacent rings rotated in the opposite sense as seen in the first four structures; structures 6 and 7 have similarly rotated rings along the chain. The seventh structure is an analogue to the sixth, with the former having improved register between amide moieties in neighboring sheets. The eighth structure contains only one chain per unit cell but with an α angle of 55° that effectively creates the axial shift between hydrogen-bonded sheets seen in the other seven structures.

IV. Conclusion

The methodology presented in the preceding section serves to generate from a priori considerations predictions for the atomistic structural detail of highly ordered polymeric solids. In addition to its suitability in representing ideal periodic structures of packed helical molecules, such as have been almost exclusively dealt with in the past, this representation provides a method by which imperfections of either a periodic or local nature may be accurately incorporated into the analysis. This additional capability becomes especially important as interest increases in polymers of a paracrystalline or polycrystalline nature. Application of this procedure to the study of a representative stiff-chain polymer, PPTA, reveals that, due to the convolution of the potential energy hypersurface, one may expect a multiplicity of viable candidates for stable geometries. In the presence of strong intermolecular packing forces, one encounters competing trends of similar magnitude, one driven by bonded interactions within a chain and the other by nonbonded interactions of the type commonly attributed to hydrogen bonds between chains. One may prioritize the development of structure according to the magnitude and specificity of interaction energies; for PPTA, the key traits are the chain stiffness arising from the rigidity of the moieties, the coplanar hydrogen bonding between chains arising from the rodlike conformation of each chain and the consequent persistent formation of sheet structures, and the relative variety of isoenergetic sheet packing geometries. It is this last feature that suggests the occurrence of several distinguishable polymorphs having comparable stability and capable of coexistence at the microscopic level. Confirmation of this behavior requires a comparison between these predictions and experimental evidence for PPTA, which is addressed in the accompanying paper.

Acknowledgment. We gratefully acknowledge the financial support of a Graduate Fellowship to G.C.R. from the National Science Foundation and grants from the Office of Naval Research and the Materials Research Laboratory at the Massachusetts Institute of Technology. Partial support of U.W.S. through the Bayer Professorship to the Department of Chemical Engineering at the Massachusetts Institute of Technology is also greatly appreciated.

Appendix. Helix Representation of Chain Conformation

The helix described entirely in terms of internal bond coordinates may be fairly simple or severely convoluted within a single helical repeat distance and there is no constraint on the rationality of the helix. We derive the corresponding helix rotation matrix $\mathbf{A}_H$ and translation vector $\mathbf{B}_H$ of Miyazawa and Sugeta[53,54] from our earlier generator matrices:

$$\mathbf{A}_H = \mathbf{Y}_k \mathbf{Y}_j^{-1} \tag{A.1}$$

$$\mathbf{B}_H = \mathbf{Y}_k \begin{bmatrix} 0 \\ 0 \\ 0 \\ 1 \end{bmatrix} - \mathbf{Y}_j \begin{bmatrix} 0 \\ 0 \\ 0 \\ 1 \end{bmatrix} \tag{A.2}$$

where

$$\mathbf{Y}_j = \mathbf{A}_1\mathbf{A}_2 \ldots \mathbf{A}_{j-1} \tag{A.3}$$

$$\mathbf{Y}_k = \mathbf{A}_1\mathbf{A}_2 \ldots \mathbf{A}_{j-1}\mathbf{A}_j \ldots \mathbf{A}_{k-1} \tag{A.4}$$

such that

$$\mathbf{X}_k^1 = \mathbf{A}_H \mathbf{X}_j^1 + \mathbf{B}_H \tag{A.5}$$

$$\mathbf{X}_j^1 = \mathbf{A}_H{}^T\mathbf{X}_k^1 - \mathbf{B}_H \quad (A.6)$$

j and k are the corresponding atoms in two successive conformational repeat units m and $m+1$, and j is greater than or equal to 3.

From $\mathbf{A}_H$ and $\mathbf{B}_H$ one can calculate the three helix parameters for a uniform, nondegenerate helix and the rotation matrix required to align the helix axis with the z axis using the equations of Sugeta and Miyazawa:

$$\mathbf{C} = (\mathbf{A}_H{}^T - \mathbf{E}_4)\mathbf{B}_H \quad (A.7)$$

$$\mathbf{C}' = (\mathbf{E}_4 - \mathbf{A}_H)\mathbf{B}_H \quad (\mathbf{E}_S \text{ is the identity matrix of order } S) \quad (A.8)$$

$$B = (\mathbf{B}_H{}^T\mathbf{B}_H)^{1/2} \quad (A.9)$$

$$C = (\mathbf{C}^T\mathbf{C})^{1/2} \quad (A.10)$$

from which it follows that

$$\cos\Theta_h = (\mathbf{C}^T\mathbf{C}')/C^2 \quad (A.11)$$

$$\rho_h = {}^1/_2 C/(1-\cos\Theta_h) \quad (A.12)$$

$$d_h = \mathbf{B}_H(\mathbf{C}^T\mathbf{C}')/(C^2\sin\Theta) \quad (A.13)$$

The coordinates may be transformed to the primary frame of reference of the helix as follows:

$$\mathbf{X}_i^h = \mathbf{T}_H\mathbf{X}_i^1 + \mathbf{D} \quad (A.14)$$

where

$$\mathbf{D} = [\rho_h \quad 0 \quad 0] \quad (A.15)$$

$$\mathbf{T}_H = \begin{bmatrix} e_1(x) & e_1(y) & e_1(z) \\ e_2(x) & e_2(y) & e_2(z) \\ e_3(x) & e_3(y) & e_3(z) \end{bmatrix} \quad (A.16)$$

$$\mathbf{e}_1 = \mathbf{C}/C \quad (A.17)$$

$$\mathbf{e}_2 = \mathbf{e}_3{}^T\mathbf{e}_1 \quad (A.18)$$

$$\mathbf{e}_3 = (\mathbf{C}^T\mathbf{C}')/C^2\sin\Theta_h \quad (A.19)$$

For the special case where $\Theta = 180°$, one must substitute an alternative calculation for the pitch and for a section of the orientation matrix:

$$\mathbf{B}_H{}^* = (\mathbf{A}_H + \mathbf{E})\mathbf{B}_H \quad (A.20)$$

$$d_h = {}^1/_2|\mathbf{B}_H{}^*| \quad (A.21)$$

$$\mathbf{e}_3 = {}^1/_2\mathbf{B}_H{}^*/d_h \quad (A.22)$$

However, in applications involving finite chain lengths, this helical coordinate conversion encounters a singularity in radius ρ_h for the degenerate straight-rod helix ($\Theta_h = 0$, $C = 0$). This singularity produces a discontinuity in helix alignment, whereby conformations infinitesimally displaced from the straight rod become sections of infinitely large spirals, with the result that alignment is rotated by 90° in space. To surmount this numerical problem, we have chosen to substitute in this vicinity of parameter space a coordinate transformation which approximates the helix axis with the major axis of the radius of gyration tensor for the finite chain segment, with a transition between the two transformations at a finite value of Θ_h. The radius of gyration tensor for the finite chain segment is calculated by using only the coordinates of the "backbone" atoms, i.e., those carbon and nitrogen atoms which lie on the backbone bond (and virtual bond) contour of the chain. Diagonalization of this tensor by successive Jacobian transformations yields the corresponding eigenvalues and eigenvectors, which correspond to the unit vectors of the principal axes of the finite chain segment. The helix is centered and aligned such that its primary axis lies along the Cartesian z axis and the secondary axis lies in the Cartesian xz plane:

$$\mathbf{X}_i^h = \mathbf{x}^T(\mathbf{r}_i - \sum_{i=1}^{N_i}(\mathbf{u}\cdot\mathbf{r}_i)/N_i) \quad (A.23)$$

$\mathbf{x}$ is the eigenvector matrix sorted such that the eigenvalues are ordered $\lambda_3 > \lambda_1 > \lambda_2$. $\mathbf{r}_i$ is the position vector of atom i, and $\mathbf{u}$ is the unit vector matrix for the Cartesian coordinate system.

This approximation allows the model to handle all cases of chain conformation in a numerically continuous manner for finite chain segments of sufficient length. However, it may readily be seen that the above transformation of coordinates is dependent upon N_i, or the length of the chain segment; this dependence becomes less sensitive as N_i increases for segments which are rodlike in conformation, since λ_3 increases faster than either λ_1 or λ_2. It does not, of course, ensure perfect alignment of the near-rod helices along their true propagation axes except in the limit of extremely large N_i.

References and Notes

(1) Brant, D. A.; Flory, P. J. *J. Am. Chem. Soc.* **1965**, *87*, 2791.
(2) Suter, U. W. *J. Am. Chem. Soc.* **1979**, *101*, 6481.
(3) Brisson, J.; Brisse, F. *Macromolecules* **1986**, *19*, 2632.
(4) Allegra, G.; Benedetti, E.; Pedone, C. *Macromolecules* **1970**, *3*, 727.
(5) Scott, R. A.; Scheraga, H. A. *J. Chem. Phys.* **1966**, *44*, 3054.
(6) Ooi, T.; Scott, R. A.; Vanderkooi, G.; Scheraga, H. A. *J. Chem. Phys.* **1967**, *46*, 4410.
(7) Tashiro, K.; Kobayashi, M.; Tadokoro, H. *Macromolecules* **1977**, *10*, 731.
(8) Bernstein, J.; Hagler, A. T. *J. Am. Chem. Soc.* **1978**, *100*, 673.
(9) Hagler, A. T.; Bernstein, J. *J. Am. Chem. Soc.* **1978**, *100*, 6349.
(10) Jorgensen, W. L.; Swenson, C. J. *J. Am. Chem. Soc.* **1985**, *107*, 569.
(11) Vacatello, M.; Avitabile, G.; Corradini, P.; Tuzi, A. *J. Chem. Phys.* **1980**, *73*, 543.
(12) Theodorou, D. N.; Suter, U. W. *Macromolecules* **1985**, *18*, 1467.
(13) Ludovice, P. J.; Suter, U. W. *Polym. Prepr. (Am. Chem. Soc., Div. Polym. Chem.)* **1987**, *28*, 295.
(14) Tripathy, S. K.; Hopfinger, A. J.; Taylor, P. L. *J. Phys. Chem.* **1981**, *85*, 1371.
(15) McCullough, R. L. *J. Macromol. Sci., Phys.* **1974**, *B9*, 97.
(16) Sorensen, R. A.; Liau, W. B.; Boyd, R. H. *Macromolecules* **1988**, *21*, 194.
(17) Sorensen, R. A.; Liau, W. B.; Kesner, L.; Boyd, R. H. *Macromolecules* **1988**, *21*, 200.
(18) Tashiro, K.; Kobayashi, M.; Tadokoro, H. *Macromolecules* **1978**, *11*, 908.
(19) Tashiro, K.; Kobayashi, M.; Tadokoro, H. *Macromolecules* **1978**, *11*, 914.
(20) Tashiro, K.; Tadokoro, H. *Macromolecules* **1981**, *14*, 781.
(21) Napolitano, R. *Macromolecules* **1988**, *21*, 622.
(22) Hopfinger, A. J.; Walton, A. G. *J. Macromol. Sci., Phys.* **1969**, *B3*, 195.
(23) Napolitano, R.; Pirozzi, B.; Tuzi, A. *Eur. Polym. J.* **1988**, *24*, 103.
(24) Saruyama, Y. *J. Chem. Phys.* **1985**, *83*, 413.
(25) Saruyama, Y.; Miyaji, H. *J. Polym. Sci., Polym. Phys. Ed.* **1985**, *23*, 1637.
(26) Flory, P. J. *Statistical Mechanics of Chain Molecules*; Interscience: New York, 1969; Chapter 1.
(27) Anand, J. N. *J. Macromol. Sci., Phys.* **1967**, *B1* (3), 445.
(28) Tashiro, K.; Kobayashi, M.; Tadokoro, H. *Macromolecules* **1977**, *10*, 413.
(29) Pertsin, A. J.; Kitaigorodsky, A. I. *The Atom–Atom Potential Method*; Cardona, M., Ed.; Springer Series in Chemical Physics 43; Springer: Berlin, 1987.
(30) Block, H.; Walker, S. M. *Chem. Phys. Lett.* **1973**, *19*, 363.
(31) Ludovice, P. L. Ph.D. Thesis, Massachusetts Institute of Technology, Cambridge, MA, 1989.

(32) Schaefgen, J. R.; Bair, T. I.; Ballou, J. W.; Kwolek, S. L.; Morgan, P. W.; Panar, M.; Zimmerman, J. In *Ultra-High Modulus Polymers*; Ciferri, A., Ward, I. M., Eds.; Applied Science: London, 1979; Chapter 6.
(33) Wilfong, R. E.; Zimmerman, J. *J. Appl. Polym. Sci., Polym. Symp.* **1977**, *31*, 1.
(34) Northolt, M. G.; Van Aartsen, J. J. *J. Polym. Sci., Polym. Symp.* **1977**, *58*, 283.
(35) Hancock, T. A.; Spruiell, J. E.; White, J. L. *J. Appl. Polym. Sci.* **1977**, *21*, 1227.
(36) Northolt, M. G. *Eur. Polym. J.* **1974**, *10*, 799.
(37) Haraguchi, K.; Kajiyama, T.; Takayanagi, M. *J. Appl. Polym. Sci.* **1979**, *23*, 915.
(38) Dobb, M. G.; Johnson, D. J.; Saville, B. P. *J. Polym. Sci., Polym. Symp.* **1977**, *58*, 237.
(39) Lifson, S.; Warshel, A. *J. Chem. Phys.* **1968**, *49*, 5116.
(40) Warshel, A.; Lifson, S. *J. Chem. Phys.* **1970**, *53*, 582.
(41) Hagler, A. T.; Huler, E.; Lifson, S. *J. Am. Chem. Soc.* **1974**, *96*, 5319.
(42) Lifson, S.; Hagler, A. T.; Dauber, P. *J. Am. Chem. Soc.* **1979**, *101*, 5111.
(43) Hummel, J. P.; Flory, J. P. *Macromolecules* **1980**, *13*, 479.
(44) Rutledge, G. C. Ph.D. Thesis, Massachusetts Institute of Technology, Cambridge, MA, 1990, Appendix C.
(45) Lauprêtre, F.; Monnerie, L. *Eur. Polym. J.* **1978**, *14*, 415.
(46) Available through the Department of Chemistry, Indiana University, Bloomington, IN, 47405, QCPE Program No. 506.
(47) Fletcher, R. A. AERE Report No. R-7125, Harwell, England; Subroutine VA10A in Harwell Subroutine Library, 1972, Harwell, England.
(48) Ladell, J.; Post, B. *Acta Crystallogr.* **1974**, *7*, 559.
(49) Schroeder, R.; Lippincott, E. R. *J. Phys. Chem.* **1957**, *61*, 921.
(50) Knoff, W. E. *J. Mater. Sci. Lett.* **1987**, *6*, 1392.
(51) Morgan, R. J.; Pruneda, C. O.; Steele, W. J. *J. Polym. Sci., Polym. Phys. Ed.* **1983**, *21*, 1757.
(52) Van Krevelin, D. W. *Properties of Polymers*; Elsevier: New York, 1972; p 88.
(53) Miyazawa, T. *J. Polym. Sci.* **1961**, *55*, 215.
(54) Sugeta, H.; Miyazawa, T. *Biopolymers* **1967**, *5*, 673.